Solidification and heat-treatment conditions affecting the tensile properties and fracture feature of an automotive AlSiMg alloy

Carolina Barbosa
Federal Institute of Education, Science and Technology of Pará-IFPA
Hugo Azevedo
Federal Institute of Education, Science and Technology of Pará-IFPA
Sharlane Costa
University of Minho
João Ribeiro
Polytechnic Institute of Bragança - IPB
José Carlos
Federal University of Pará-UFPA
Thiago Costa
Federal Institute of Education, Science and Technology of Pará-IFPA
Otávio Rocha (otavio.rocha@ifpa.edu.br)
Federal Institute of Education, Science and Technology of Pará-IFPA

Research Article

Keywords: Transient solidification, Heat treatment, Microstrutcure, Fracture, Tensile properties

Posted Date: January 17th, 2023

DOI: https://doi.org/10.21203/rs.3.rs-2393305/v1

Additional Declarations: No competing interests reported.

Version of Record: A version of this preprint was published at Silicon on March 18th, 2023. See the published version at https://doi.org/10.1007/s12633-023-02409-3.

Abstract

In this work, a study on the interrelationship between the solidification and heat-treatment processes parameters with tensile properties and fracture feature was performed with an automotive AlSiMg alloy. For that, samples of the horizontally solidified Al7Si0.3Mg (wt.%) alloy were subjected to the T6-heat treatment as well as tensile tests were performed on both investigated samples, under conditions established from the literature. The solidification conditions such as growth and cooling rates and the secondary dendritic spacing (V_L and T_R and λ_2, respectively) and their effects on the ultimate tensile strength (σ_{UTS}) and elongation (E%) were evaluated. It was observed higher σ_{UTS} values in the heat-treated samples and finer microstructures have inherited a better E% performance. Analysis by SEM/EDS fractography on both samples showed a mix between brittle and ductile fractures, constituted by cleavage facets, secondary cracks, facets covered with micro-voids, tear ridges and dimples. It has allowed deducing on the occurrence of a transition from ductile to brittle fracture along the solidified ingot as well as the predominance of brittle fracture in the heat-treated samples.

Introduction

The use of metallic alloys in the various sectors of engineering and industry is based mainly on mechanical properties, since very well programmed, the products produced by these alloys are able to withstand the loads that are subjected when in service [1]. It is known that these properties depend largely on the structure which is closely related to chemical compositions and processing conditions, among which heat treatment is among the most used [1]. Heat treatments of metallic alloys are accredited as one of the most important methods of materials manufacturing and developing of new technologies throughout human history. Through controlled heating and cooling operations, the materials properties undergo considerable variations as a result of changes in macrostrutcture and microstructure characteristics [1].

Grain refinement, dissolution of secondary phases, distribution and morphology changes of phases have been studied over the decades and are linked to the enhancement of mechanical properties in heat treated aluminum alloys [2–6]. Shivkumar, Apelian and collaborators [5, 7, 8] studying Al-Si-Mg alloys observed that heat treatment changes silicon morphology and that the kinetics of spheroidization are affected by the as-cast microstructure. Similarly, addition of sodium, strontium, antimony and bismuth has been investigated as a method of chemical modification of Si-crystal, and studies indicate that machinability, tribology and mechanical properties are significantly affected [9–16].

Recent studies reported that the microstructure scale of as-cast ingots directional solidified has effects on heat treatment parameters, and plays a crucial role in the extent of morphological transition of the undissolved phases from acicular to spheroidized in aluminum alloys [17, 18]. In a previous works published by the authors regarding AlSiMg automotive alloy subjected to T6-heat treatment, were stated that spheroidized-like eutectic Si particles and Chinese script iron-rich phase were favored after heat

treatment in refined microstructure scale conditions, resulting in different behaviors between as-cast and HT samples subjected to responses to microhardness and wear resistance [6, 19].

Microstructural scale, phases morphology and heat treatment are conducive to change the properties of automotive AlSiMg alloy separately or in conjunction with each other, to develop desired and optimum properties in the casting. In this regard, a series of works were recently developed with the automotive casting Al7Si0.3Mg (wt.%) alloy, which in a first stage aimed to analyze the effects of solidification conditions on the microstructure and mechanical properties [20–23]. In this step, the influence of the thermal solidification parameters, such as growth and cooling rates on the length of the dendritic microstructure as well as on the size, distribution and morphology of the Mg_2Si/Fe intermetallic compounds (ICMs) and, in turn, on the hardness and tensile properties were investigated. In a second stage [6, 19, 24], T6 heat treatment under different conditions has been applied to the as-cast samples resulting from the work of References [20–23].

Chen et al. [20] and Lima et al. [21] obtained as-cast ingots of the Al7Si0.3Mg alloy (wt.%) resulting from sand molds and transient horizontal solidification, respectively. The typical solidification microstructure observed by both works consisting of a dendritic network with Al-rich primary and secondary phases (Al_α, Si crystals and IMCs). It has been observed finer dendritic microstructures for higher cooling rates values. From the as-cast samples obtained by Lima et al [21], Souza et al. [22] and Barbosa et al. [23], analyzes on the influence of the solidification parameters on the microhardness (HV) of the aforementioned alloy have been performed. In addition, Souza et al. [22] evaluated the Mg and Cu addition in the Al-7Si alloy (wt.%), depicted higher HV values for the ternary Al-7Si-(0.3Mg;3Cu) alloys (wt.%), while Barbosa et al. [23] noted higher HV values on ICMs and Si crystals in relation to the Al-rich primary phase (Al_α).

More recently, comparative studies on solidification and T6-heat treatment conditions in Al-7Si-xMg (wt.%) cast aluminum alloys have been carried out [6, 18, 19, 24]. Barbosa et al. [6] and Azevedo et al. [19] analyzed the interrelation between the horizontal solidification and treatment processes parameters on the microhardness and wear performance from the work of References [22, 23]. Chen et al. [24] developed investigations to analyze the influence of Mg composition and heat treatment conditions on the mechanical properties of Al-7Si-xMg cast aluminum alloys ($x \cong 0.26$, 0.4 and 0.58 wt.%). In this sense, the present work is a continuity of investigations [6, 18, 21–23] which, although broad, still left a large gap in terms of a more complete mechanical analysis and, thus, aims to present a study on the correlation between tensile properties and microstructural parameters and fracture feature before and after thermal treatment by T6.

Experimental Procedure

In this work, an Al7Si0.3Mg alloy ingot (wt.%) was obtained by means of a horizontal water-cooled solidification device. Figure 1 shows a complete assembly scheme of the furnace used in the solidification experiments. Experimental temperature curves were obtained and used to determine the solidification thermal parameters, such as growth and cooling rates (V_L and T_R, respectively). Additional

details on the operational procedures of the experiments can be consulted in our recently published works [6, 19, 21–23].

In our recent works [6, 19], the precipitation treatment by T6 has been carried out on as-cast samples of the horizontally solidified investigated alloy under the same conditions of this work. It is important to emphasize that the operational parameters for application of the T6-thermal treatment followed guidelines of ASTMB-597-92 - Standard Practice for Heat Treatment of Aluminum Alloys, that is: solution treating performed during 3 h at 520 ± 2°C, followed by quenching in warm water (70 ± 2°C), aging for 1, 2, 3, and 4 h at 155 ± 2°C and air-cooling, as shown by the thermal cycles in Fig. 2.

Specimens for tensile tests were prepared from the as-cast ingot, as shown in Fig. 2. In order to guarantee the reproducibility of the results, six samples were prepared for each position, three for analysis of the solidification conditions (V_L, T_R and λ_2) and the other three to evaluate the heat treatment conditions. Thus, from the six as-cast specimens, three were submitted to the T6 -treatment, according to the thermal cycle of Fig. 3, considering the aging time equal to 3h, since the highest microhardness value (HV) was obtained for this condition [6]. The tests were carried out according to ASTM standards: E384/11 and E8M/04. They have been conducted with a strain rate 0.05 mm $s^{-}1$ [29] and the investigated properties include ultimate tensile strength (σ_{UTS}) and elongation (E%).

In turn, as-cast and heat treated samples were subjected to microstructural characterization. The length of the microstructural scale was analyzed using secondary dendritic spacing (λ_2). Once the λ_2 values were measured, following the technique from the literature [20, 21], they were correlated with solidification parameters and tensile properties of both investigated samples. Image processing MOTIC system and the Image J software were used to measure the secondary dendrite arm spacings (~ 20) independent readings for each selected position. A scanning electron microscope (SEM TESCAM,VEGA LMU) coupled to an energy dispersion spectrum (EDS X-MAX 20, Oxford) was used to investigate fracture feature of both as-cast and heat treated specimens.

Results And Discussion

It is known that the thermal parameters have an effect on the length of the microstructural scale. It has been evaluated by the experimental results achieved considering the solidification conditions assumed in the present work, such as the growth and cooling rates (V_L and T_R, respectively). They were obtained from experimental data resulting from horizontal solidification, as presented in Fig. 4a, which in turn were used to determine the values, varying with the position in the as-cast ingot, as shown in Fig. 4b. It is clearly observed that the cooled mold imposes high V_L and T_R values close to the heat transfer interface, which decrease with the increasing formation of the solid layer. Mathematical power equations given by the general expression $A.P^{-a}$ characterize the V_L and T_R variation with the position in the as-cast ingot. This significantly influenced the dendritic network, inheriting finer dendritic microstructures for higher V_L and T_R values, as can be seen in Fig. 4c. As observed, it has been represented by experimental power

expressions in the forms of Constant. $V_L^{-2/3}$ and Constant.$T_R^{-1/3}$, which characterize the λ_2 coarsening laws with the solidification thermal parameters.

In our works [6, 19, 21, 23] the λ_2 values were measured from the cooled interface, in both as-cast and heat-treated samples, processed under the same conditions assumed in the present work. The expressions resulting from the investigations, which characterize the growth laws of λ_2 of the aforementioned samples are presented in Fig. 5. It was observed that the heat treatment affected the length of the dendritic microstructure scale, since the λ_2 values came be greater in the treated samples by T6, as seen in Fig. 5a. It was also observed that finer microstructures contributed to the dissolution of the Mg_2Si-intermetallic compound within the Al-rich matrix [6, 19, 24], as well as potentiated the spheroidization process of the eutectic Si crystals during the solution treatment, as depicted by the microstructures above the graph in Fig. 5. Finer microstructures have also allowed better dissolution of Al_2Cu and obtaining spherical-like Si particles during Treatment by T6 in AlSiCu alloys [17, 18, 27, 29].

Figures 6 and 7 present, for both investigated specimens, the results obtained from the tensile tests for two as-cast and heat-treated samples from the heat transfer surface, and studied mechanical properties, respectively. Higher mechanical strengths were achieved for heat-treated samples, as can be seen in Figs. 6a and 6b. It is observed that the analyzed properties performance along the position in the ingot has not allowed to obtain a mathematical relationship as a function of the solidification parameters (V_L, T_R e λ_2), especially for the σ_{UTS} values, as seen in Fig. 6a, although finer solidification microstructures have inherited a slight improvement in deformation (E%), as noted in Fig. 6b. This has induced to calculate for both studied samples a resulting average value from all the averages of each position, as shown in Fig. 6c. It can be observed high σ_{UTS} and E% values for heat-treated samples, that is, increases from 132 to 194 MPa (≅47%) and 5.8 to 6% (≅5.5%) have been achieved with the heat treatment, confirming the precipitation hardening without deleterious effects on the deformation. In general, the increase in mechanical resistance achieved with heat treatment does not cause damage to deformation, as can be seen in Fig. 6c. Precipitation hardening also have been observed in the results of HV from the work of Reference [20] for the horizontally solidified and heat-treated Al7Si0.3Mg alloy in the same conditions of this work.

However, Souza et al. [29] have established an inverse mathematical relationship of σ_{UTS} and E% with λ_2 for the horizontally solidified Al7Si3Cu alloy, that is, they have observed higher σ_{UTS} and E% values for smaller secondary dendrite arm spacing, but HV and yield strength (σ_{YS}) did not vary with λ_2. In turn, Sousa et al. [18] have submitted samples of the horizontally solidified Al7Si3Cu alloy to the T6 heat treatment and observed the hardening of the alloy as well as higher HV values with increasing aging time. Chen et al. [24] have reported higher σ_{UTS}, σ_{YS} and E% values for finer microstructures in as-cast samples and heat treated by T6 of Al7SixMg alloys, also observing higher values of the aforementioned mechanical properties after heat treatment, as well as proposing an inverse mathematical relationship of σ_{UTS}, σ_{YS} and E% with a function of λ_2

Also in a recent study [19], a reversal wear characteristics was observed in as-cast samples of the Al7Si0.3Mg alloy (wt.%) treated by T6, since lower wear volume and rate values were found for finer as-cast microstructures, while the heat-treated microstructures showed the best wear conditions. It has been attributed mainly to the higher λ_2 values reported in samples subjected to heat-treatment, as seen in Fig. 5a, as well as the greater amount of spherical-like Si particles for refined microstructures, as noted in Fig. 5b. In addition, the collapse of tertiary dendritic branches during solution treatment as well as the higher global hardness value for greater λ_2 also seems to have contributed [19]. Thus, in verification to the results of E%, shown in Fig. 6b, in which the finer heat-treated microstructures have the lowest E% value, combined with the analysis from the author's work [19] on reverse wear parameters performance, it can be deduced that there is an agreement between the results. Ache et al. [28] have depicted better conditions of wear and mechanical properties for finer as-cast and T6-heat treated microstructures of upward solidified Al2MgZn alloys, but they have highlighted that depending on the microstructure features and the contact aspects of the tribological system the wear resistance can have an opposite behaviour, inducing inadequate selection of material condition.

Figures 8 and 9 show the SEM images and element scans mapping by EDS of the fractured areas for two as-cast and heat-treated samples, revealed in two samples solidified under different solidification thermal parameters conditions. In general, it is observed that the features of all fracture surfaces of the studied samples are indicate a mix between brittle and ductile fractures, constituted by cleavage facets, secondary cracks, facets covered with micro-voids, tear ridges and dimples. In addition, the Mg_2Si/IMCs-like Mg element, initially segregated within the interdendritic regions of the as-cast samples, as noted by scan mappings in Figs. 8a and 9a, has been completely and uniformly dissolved in the Al-rich matrix during the solution treatment, as can be verified in Figs. 8b and 9b as well as has been reported in our works [6, 19]. It also can be observed by the scan mappings of both investigated samples fibrous-like Si crystals and finer and distributed better Fe-ICMs in position of the ingot near the cooled base, that is, for solidification conditions of high cooling rates and lower λ_2 value, as noted in Figs. 7a and 8a.

Regarding morphology and fracture modes analysis from the SEM fractographies of as-cast regions, have allowed to evidence the predominance and the better distribution of small dimples against cleavage facet regions in position close to the heat-transfer surface, deducing the occurrence of a transition from ductile to fragile fracture with decreasing cooling rate as well as with increasing secondary dendritic spacing, as seen in Figs. 8a and 9a, respectively. This fracture feature can be associated by the elongation performance observed along the as-cast ingots, since higher and lower E% values have been obtained for positions near and far from the refrigerated base, respectively, as reported in Fig. 6b. Souza et al. [29] also reported for the horizontally solidified Al7Si3Cu alloy (wt.%) a transition from ductile to brittle fracture along the position of the as-cast ingot, attributing the authors to the decrease in T_R as well as the increase in λ_2. Chen et al. [24] have depicted that the increase in the cooling rate and, consequently, the refinement of the dendritic microstructure, cause transitions in both fracture path from transgranular to intergranular as well as in the fracture mode from quasi-cleavage for dimple.

In turn, the presence of dominant cleavage regions is observed in the heat-treated fractured samples, as seen in Figs. 8b and 9b, allowing to admit the predominance of brittle fracture in both analyzed positions. It has been observed more extensive cleavage areas in the furthest position from the cooled base, as noted in Fig. 8b. This has inherited a deformation behavior similar to that observed in as-cast samples, i.e., lower E% values have been achieved in heat-treated positions far from the heat-transfer surface.

Conclusion

The main conclusions obtained from this study are:

1. Ultimate tensile strength values were achieved for heat-treated samples, proving the effectiveness of heat treatment under the assumed conditions. Despite the hardening of the Al-rich matrix, this has not influenced the elongation performance, since in general the E% values remained very close in both investigated samples, even being slightly better.
2. Under the assumed conditions, finer microstructures have inherited better deformation conditions for both solidification and heat-treatment samples.
3. Analysis from the SEM/EDS fractrographs of both as-cast and heat-treated samples has shown a perfect dissolution of the Mg_2Si-IMCs in the matrix during the solution heat treatment. In addition, EDS scan mappings have depicted finer Si and Fe particles in a-cast samples, for higher and lower T_R and λ_2 values, respectively. This has inherited better conditions for obtaining spherical-like Si crystals after the solution treatment and probably contributed to the good E% performance.
4. From the analysis of fracture features performed on both as-cast and heat-treated samples, it was observed by the fracture morphologies in the as-cast samples the predominant presence of dimples and cleavage for finer and coarser microstructures, respectively, deducing the occurrence of a transition from ductile to brittle fracture modes along the length of the ingot. While in samples treated by T6, cleavage areas became prominent, suggesting a predominance of brittle fracture.

Declarations

Acknowledgements

The authors acknowledge the support provided by IFPA - Federal Institute of Education, Science and Technology of Pará - Campus Belém, to the Polytechnic Institute of Bragança for the master's degree and international exchange of the student Carolina Rizziolli Barbosa, respectively, and UFPA - Federal University of Pará.

Funding

The authors listed below are grateful for the financial support provided by the following foundations:

1. Otávio Fernandes Lima da Rocha: CNPq - National Council for Scientific and Technological Development (Grants 302846/2017-4).

2. Sharlane Costa and João Ribeiro: Foundation for Science and Technology (FCT, Portugal) for financial support by national funds FCT/MCTES to CIMO (UIDB/00690/2020).

Competing Interests

The authors have no relevant financial or non-financial interests to disclose.

Author Contributions

All authors contributed to the study conception and design. Material preparation, data collection and analysis were performed Carolina Rizziolli Barbosa, Hugo André Magalhães de Azevedo, Sharlane Costa, João Eduardo Pinto Castro Ribeiro, José Carlos de Araújo Cardoso Filho, Thiago Antônio Paixão de Sousa Costa, and Otávio Fernandes Lima da Rocha. The first draft of the manuscript was written by Otávio Fernandes Lima da Rocha and all authors commented on previous versions of the manuscript. All authors read and approved the final manuscript.

References

1. Chiaverini V (2003) Tratamento térmico das ligas metálicas. Associação Brasileira de Metalurgia e Materiais, São Paulo
2. Onurlu S, Tekin A (1994) Effect of heat treatment on the insoluble intermetallic phases present in an AA 6063 alloy. J. Mater Sci. https://doi.org/10.1007/BF00368940
3. Sjölander E, Seifeddine S (2010) The heat treatment of Al–Si–Cu–Mg casting alloys. J Mater Process Technol. https://doi.org/10.1016/j.jmatprotec.2010.03.020
4. Marioara CD, Andersen SJ, Jansen J, Zandbergen HW (2003) The influence of temperature and storage time at RT on nucleation of the β phase in a 6082 Al–Mg–Si alloy. Acta Mater. https://doi.org/10.1016/S1359-6454(02)00470-6
5. Apelian D, Shivkumar S, Sigworth G (1989) Fundamental aspects of heat treatment of cast Al-Si-Mg alloys. AFS Trans. 97:727-742.
6. Barbosa CR, Machado GH, Azevedo HM, Rocha FS, José Filho C, Pereira AA, Rocha OL (2020) Tailoring of processing parameters, dendritic microstructure, Si/intermetallic particles and microhardness in as-cast and heat-treated samples of Al7Si0.3Mg alloy. Met. Mater. Int. https://doi.org/10.1007/s12540-019-00334-y
7. Shivkumar S, Ricci Jr S, Apelian D (1990) Influence of solution parameters and simplified supersaturation treatments on tensile properties of A356 Alloy. AFS Trans. 98:913-922.
8. Shivkumar S, Ricci Jr S, Steenhoff B, Apelian D, Sigworth G (1989) An experimental study to optimize the heat treatment of A356 alloy. AFS Trans. 97:791-810.
9. Bian XF, Wang WM, Qin JY (2000) Structures of liquid Al-Si alloy modified by Sr. Mater. Sci. Forum. https://doi.org/10.4028/www.scientific.net/MSF.331-337.349

10. Liao H, Sun Y, Sun G (2002) Correlation between mechanical properties and amount of dendritic α-Al phase in as-cast near-eutectic Al–11.6% Si alloys modified with strontium. Mater. Sci. Eng. A. https://doi.org/10.1016/S0921-5093(01)01949-9
11. Shivkumar S, Ricci S, Keller C, Apelian D (1990) Effect of solution treatment parameters on tensile properties of cast aluminum alloys. J. Heat Treat. https://doi.org/10.1007/BF02833067
12. Farahany S, Ourdjini A, Idris MH, Thai LT (2011) Effect of bismuth on microstructure of unmodified and Sr-modified Al-7Si-0.4 Mg alloys. Trans. Nonferrous Met. Soc. China. https://doi.org/10.1016/S1003-6326(11)60881-9
13. Dias M, Oliveira R, Kakitani R, Cheung N, Henein H, Spinelli JE, Garcia A (2020) Effects of solidification thermal parameters and Bi doping on silicon size, morphology and mechanical properties of Al-15wt.%Si-3.2wt.%Bi and Al-18wt.%Si-3.2wt.%Bi alloys. J. Mater. Res. Technol. https://doi.org/10.1016/j.jmrt.2020.01.083
14. Costa TA, Dias M, Silva C, Freitas E, Silva AP, Cheung N, Garcia A (2019) Measurement and interrelation of length scale of dendritic microstructures, tensile properties, and machinability of Al-9wt%Si-(1wt%Bi) alloys. Int. J. Adv. Manuf. Technol. https://doi.org/10.1007/s00170-019-04211-1
15. Farahany S, Ourdjini A, Bakar TA, Idris MH (2014) Role of bismuth on solidification, microstructure and mechanical properties of a near eutectic Al-Si alloys. Met. Mater. Int. https://doi.org/10.1007/s12540-014-5019-5
16. Wu X, Zhang G, Wu F (2013) Influence of Bi addition on microstructure and dry sliding wear behaviors of cast Al-Mg2Si metal matrix composite. Trans. Nonferrous Met. Soc. China. https://doi.org/10.1016/S1003-6326(13)62627-8.
17. Costa TA, Dias M, Gomes LG, Rocha OL, Garcia A (2016) Effect of solution time in T6 heat treatment on microstructure and hardness of a directionally solidified Al–Si–Cu alloy. J. Alloys Compd. https://doi.org/10.1016/j.jallcom.2016.05.099
18. Souza FA, Costa MO, Magno IA, Nascimento JM, Silva AP, Costa TS, Rocha OL (2019) Investigation on microstructural and microhardness evolution in as-cast and T6/heat-treated samples of a horizontally solidified AlSiCu alloy. J. Mater. Res. Technol. https://doi.org/10.1016/j.jmrt.2019.06.054
19. Azevedo HM, Botelho TM, Barbosa CR, Sousa AP, Costa TA, Rocha OL (2020) Study of drywear behavior and resistance in samples of a horizontally solidified and T6/heat-treated automotive AlSiMg alloy. Tribol. https://doi.org/10.1007/s11249-020-01302-z
20. Chen R, Shi Y, Xu Q, Liu B (2014) Effect of cooling rate on solidification parameters and microstructure of Al- 7Si- 0.3 Mg- 0.15 Fe alloy. Trans. Nonferrous Met. Soc. China. https://doi.org/10.1016/S1003-6326(14)63236-2
21. Lima JO, Barbosa CR, Magno IAB, Nascimento JM, Barros AS, Oliveira MC, Souza FA, Rocha OL (2018) Microstructural evolution during unsteady-state horizontal solidification of Al-Si-Mg (356) alloy. Trans. Nonferrous Met. Soc. China. https://doi.org/10.1016/S1003-6326(18)64751-X

22. Souza F, Lima J, Rizziolli C, Magno I, Barros A, Moreira A, Rocha O (2018) Microstructure and microhardness in horizontally solidified Al–7Si–0.15 Fe–(3Cu, 0.3 Mg) alloys. Mater. Sci. Technol. https://doi.org/10.1080/02670836.2018.1444923
23. Barbosa CR, Lima JOM, Machado GMH, Azevedo HAM, Rocha FS, Barros AS, Rocha OFL (2019) Relationship between aluminum-rich/intermetallic phases and microhardness of a horizontally solidified AlSiMgFe alloy. Mater. Res. https://doi.org/10.1590/1980-5373-MR-2018-0365
24. Chen R, Xu Q, Guo H, Xia Z, Wu Q, Liu B (2017) Correlation of solidification microstructure refining scale, Mg composition and heat treatment conditions with mechanical properties in Al-7Si-Mg cast aluminum alloys. Mater. Sci. Eng. A. https://doi.org/10.1016/j.msea.2016.12.051
25. Çadırlı E (2013) Effect of solidification parameters on mechanical properties of directionally solidified Al-rich Al-Cu alloys. Met. Mater. Int. https://doi.org/10.1007/s12540-013-3006-x
26. Nascimento MS, Franco ATR, Frajuca C, Nakamoto FY, Santos GAD, Couto AA (2018) An experimental study of the solidification thermal parameters influence upon microstructure and mechanical properties of Al-Si-Cu alloys. Mater. Res. https://doi.org/10.1590/1980-5373-MR-2017-0864
27. Magno IA, Souza FA, Costa MO, Nascimento JM, Silva AP, Costa TS, Rocha OL (2019) Interconnection between the solidification and precipitation hardening processes of an AlSiCu alloy. Mat. Sci. Technol. https://doi.org/10.1080/02670836.2019.1591028
28. Ache C, Lopes M, Reis B, Garcia A, Santos CD (2020) Dendritic spacing/columnar grain diameter of Al–2Mg–Zn alloys affecting hardness, tensile properties, and dry sliding wear in the as-cast/heat-treated conditions. Adv. Eng. Mater. https://doi.org/10.1002/adem.201901145
29. Souza FA, Magno IA, Costa MO, Barros AS, Nascimento JM, Carvalho DB, Rocha OL (2019) Unsteady-state horizontal solidification of an Al–Si–Cu–Fe alloy: relationship between thermal parameters and microstructure with mechanical properties/fracture feature. Met. Mat. Int. https://doi.org/10.1007/s12540-018-0174-8

Figures

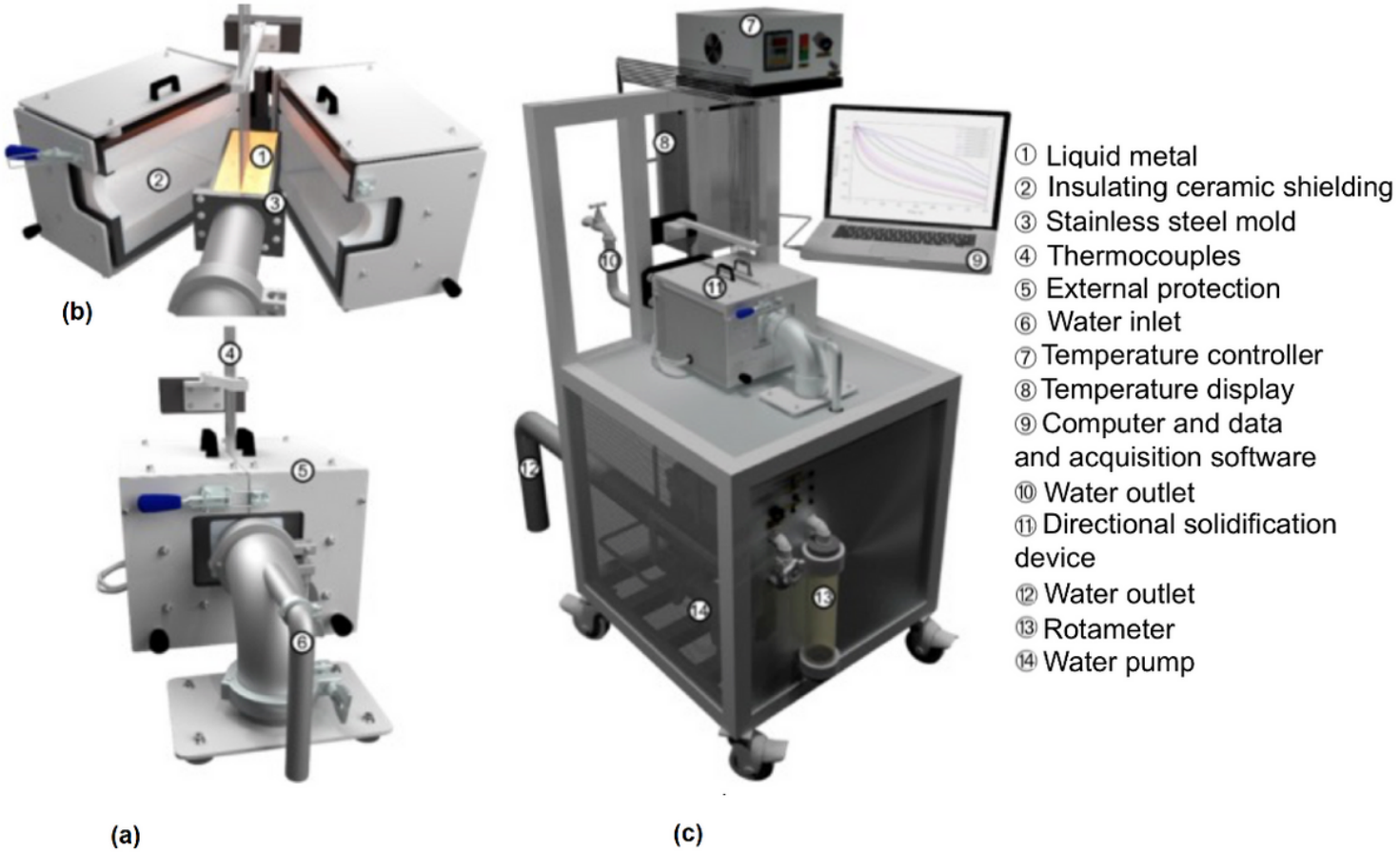

Figure 1

Details of the solidification furnace: (a) and (b) horizontal solidification device showing the water injection system, ingot mold and thermocouples and (c) complete assembly of the horizontal solidification furnace.

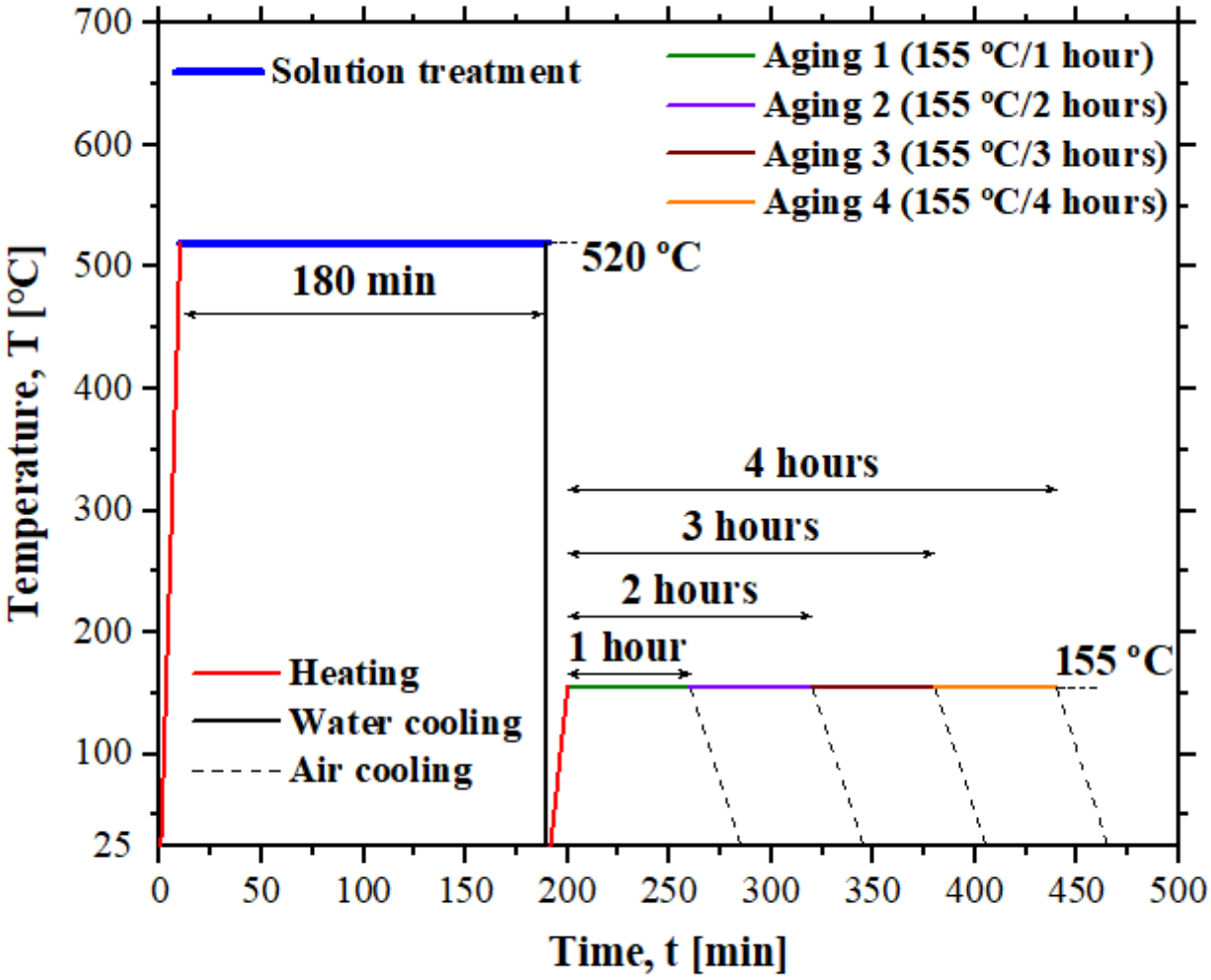

Figure 2

Thermal cycle showing the operational parameters of the three stages of the T6 -treatment.

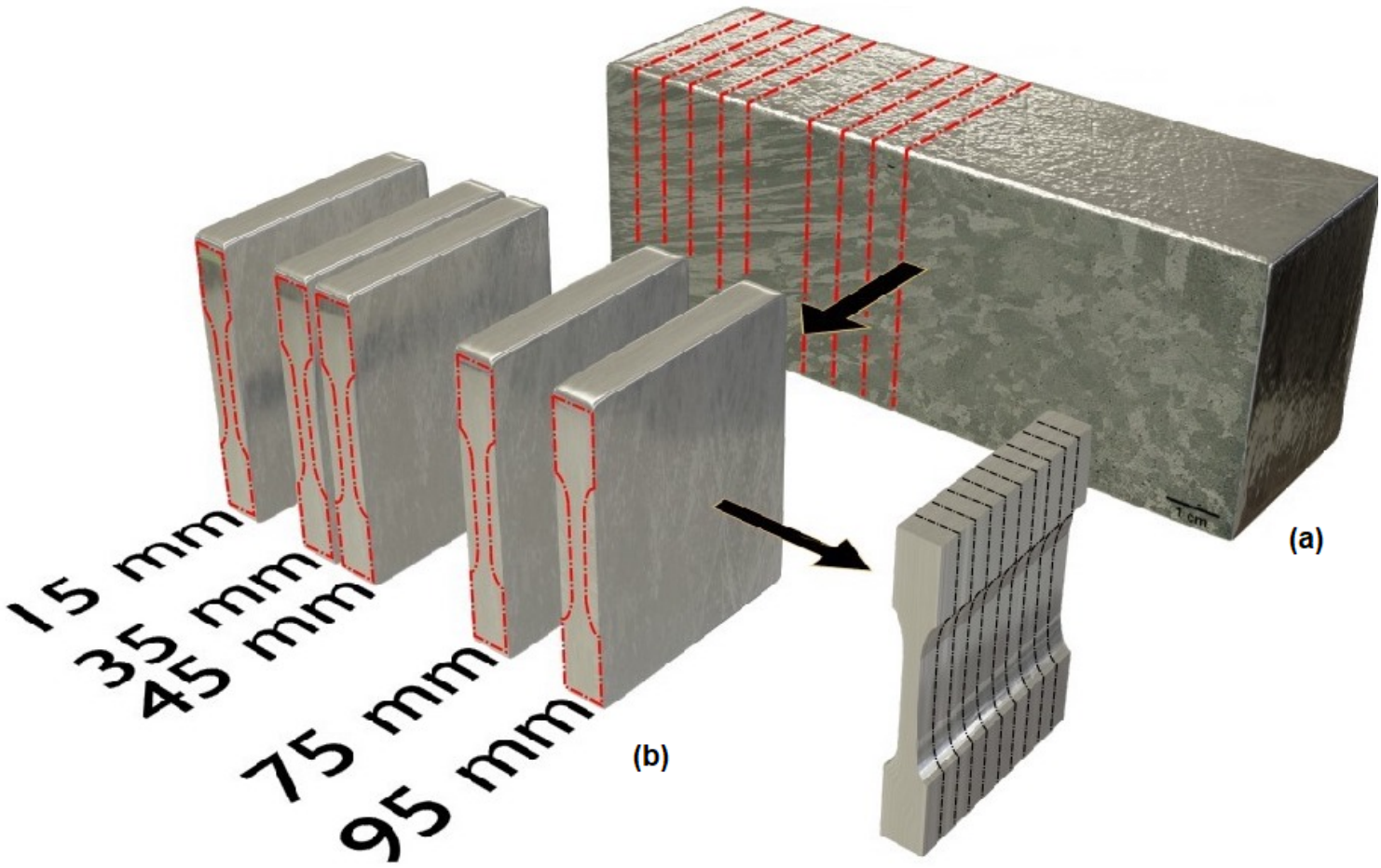

Figure 3

(a) As-cast ingot of the investigated alloys, resultant from the solidification process and (b) cheme of sample removal from the ingot resulting for tensile tests.

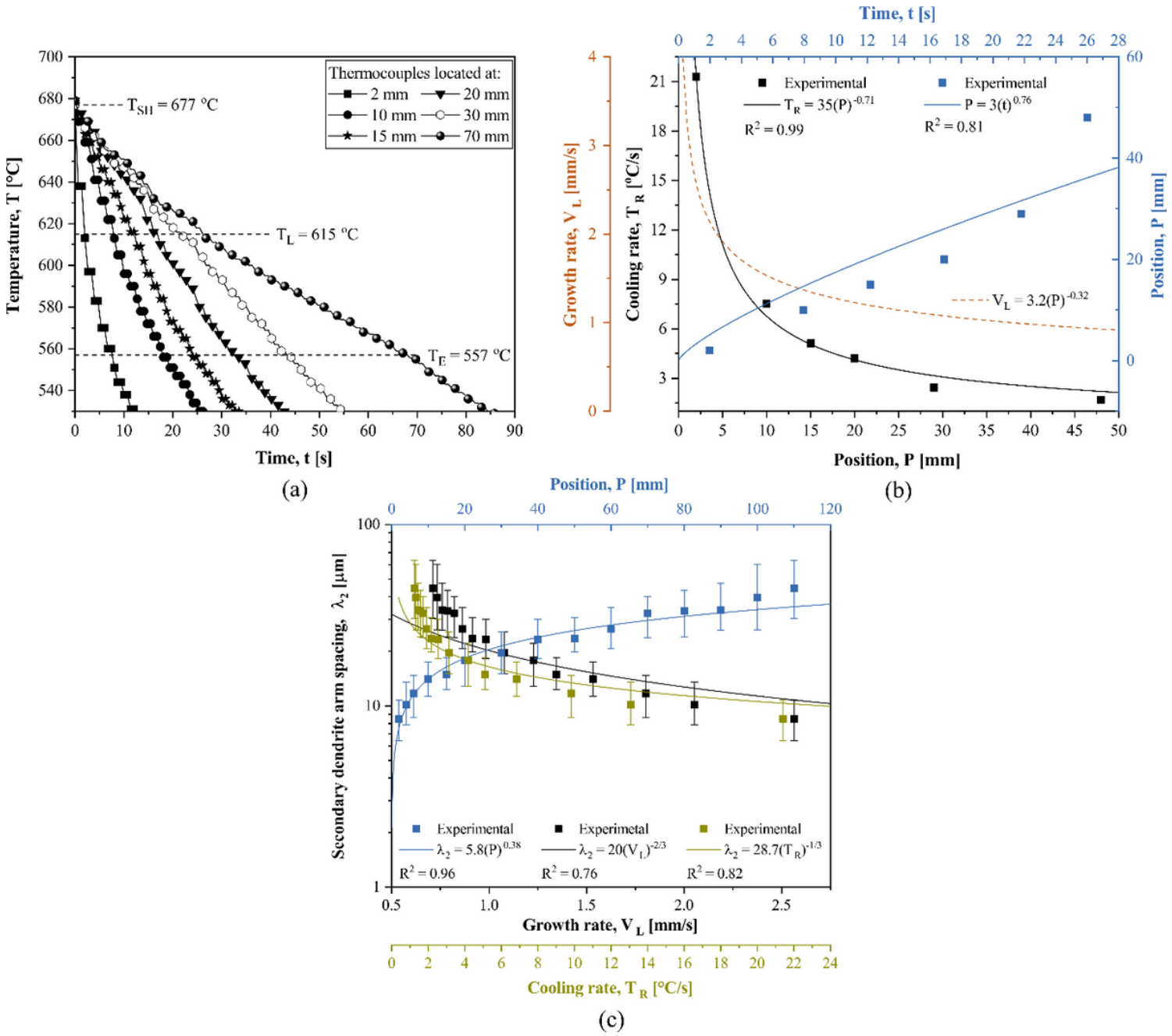

Figure 4

process: (a) experimental temperature curves for 6 thermocouples from the heat -transfer interface, (b) Growth and cooling rates (V_L and T_R), and (c) secondary dendritic spacing (λ_2) as a function of the position in the ingot, V_L and T_R.

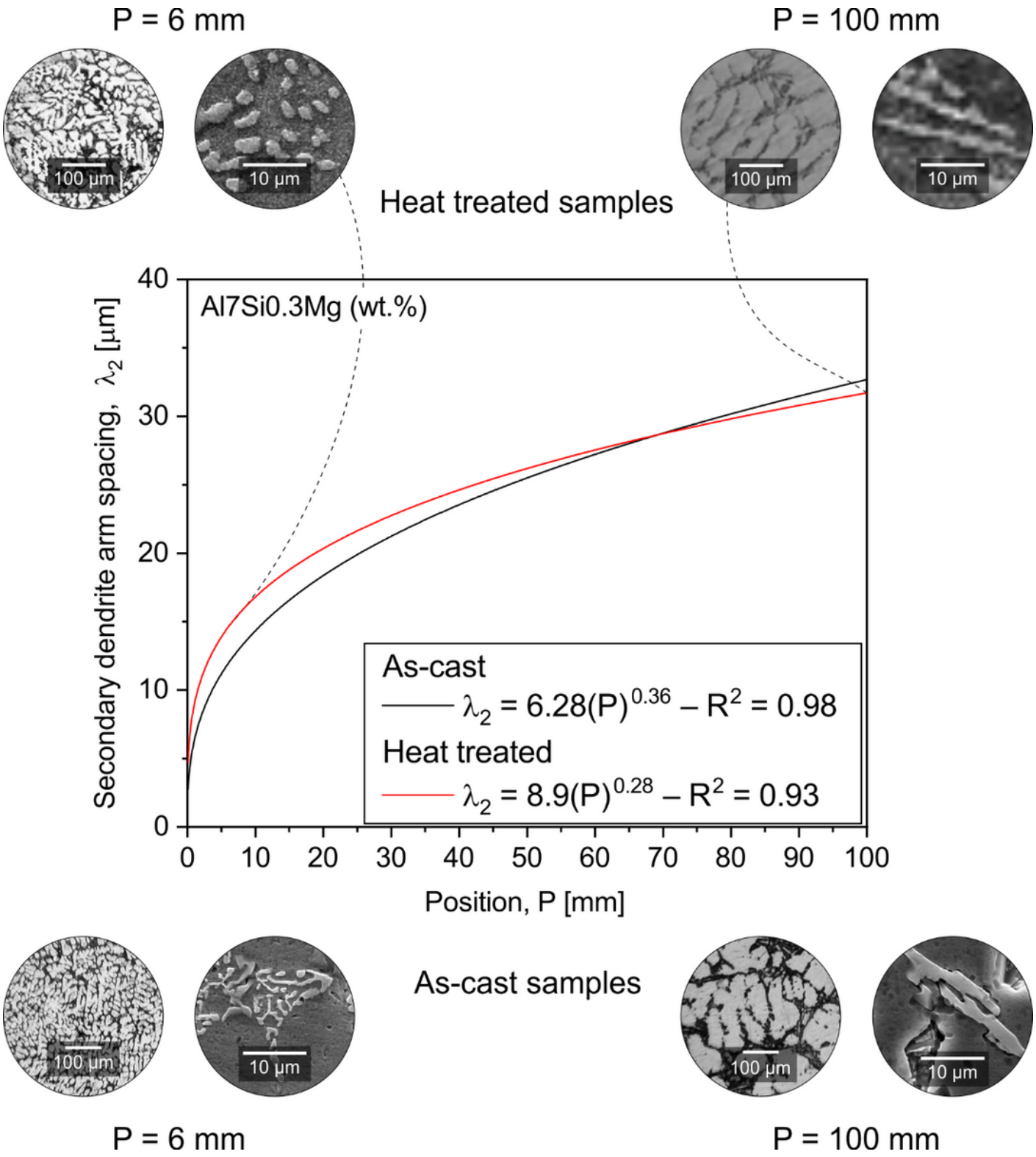

Figure 5

Comparative curves of λ_2 evolution for both analyzed samples, showing microstructural evolution for two positions from the cooled base.

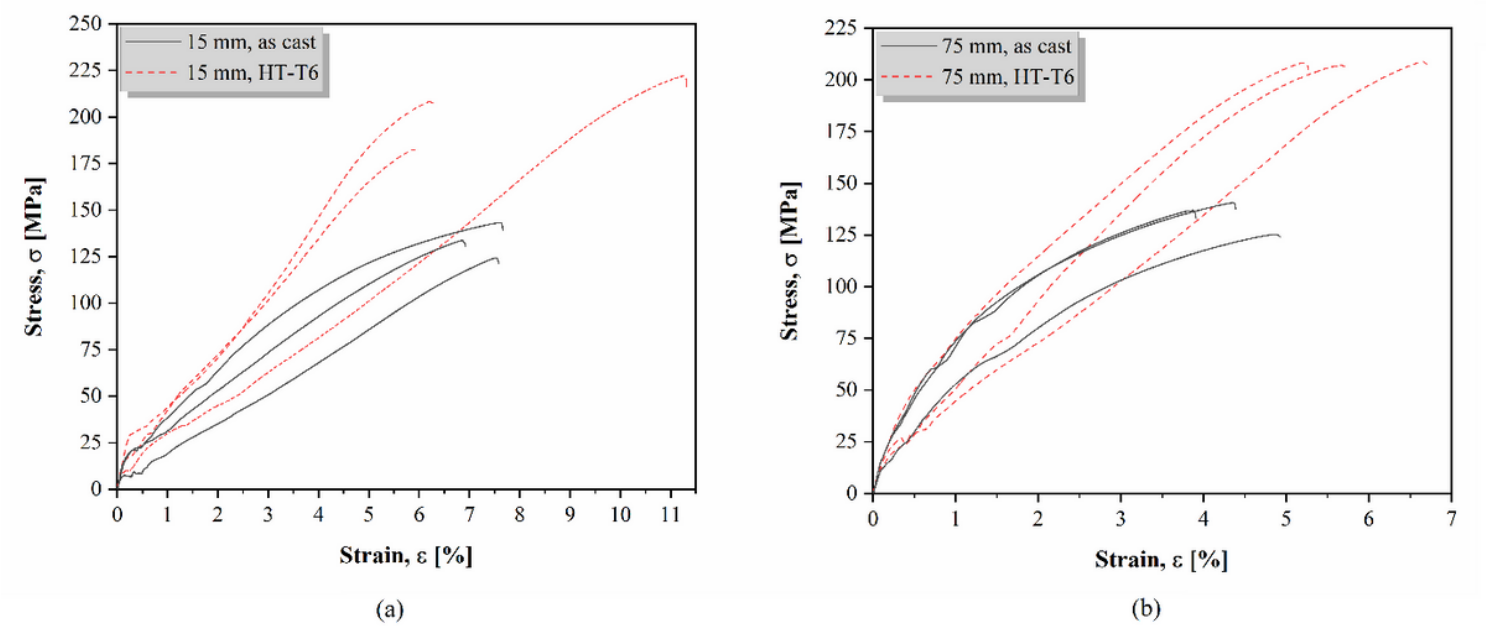

Figure 6

Stress x Strain diagrams for two as-cast and heat-treated samples in positions from the cooled base: (15) mm and (b) 75mm.

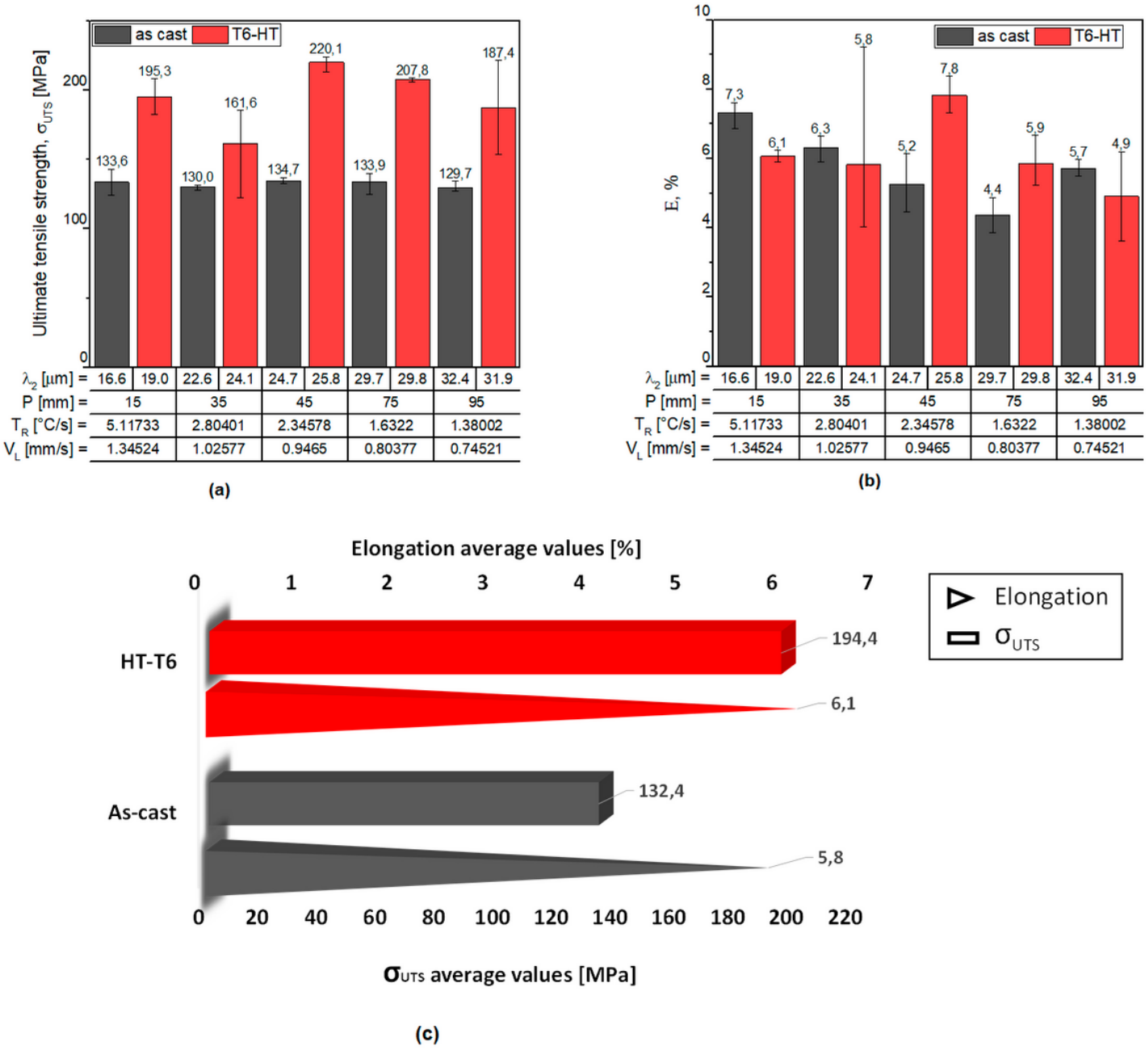

Figure 7

Experimental results of the studied properties resulting from the tensile tests: (a) and (b) ultimate tensile strength and elongation vs. solidification parameters, respectively and (c) resulting average values of ultimate tensile strength and elongation, calculated for all position of both investigated samples.

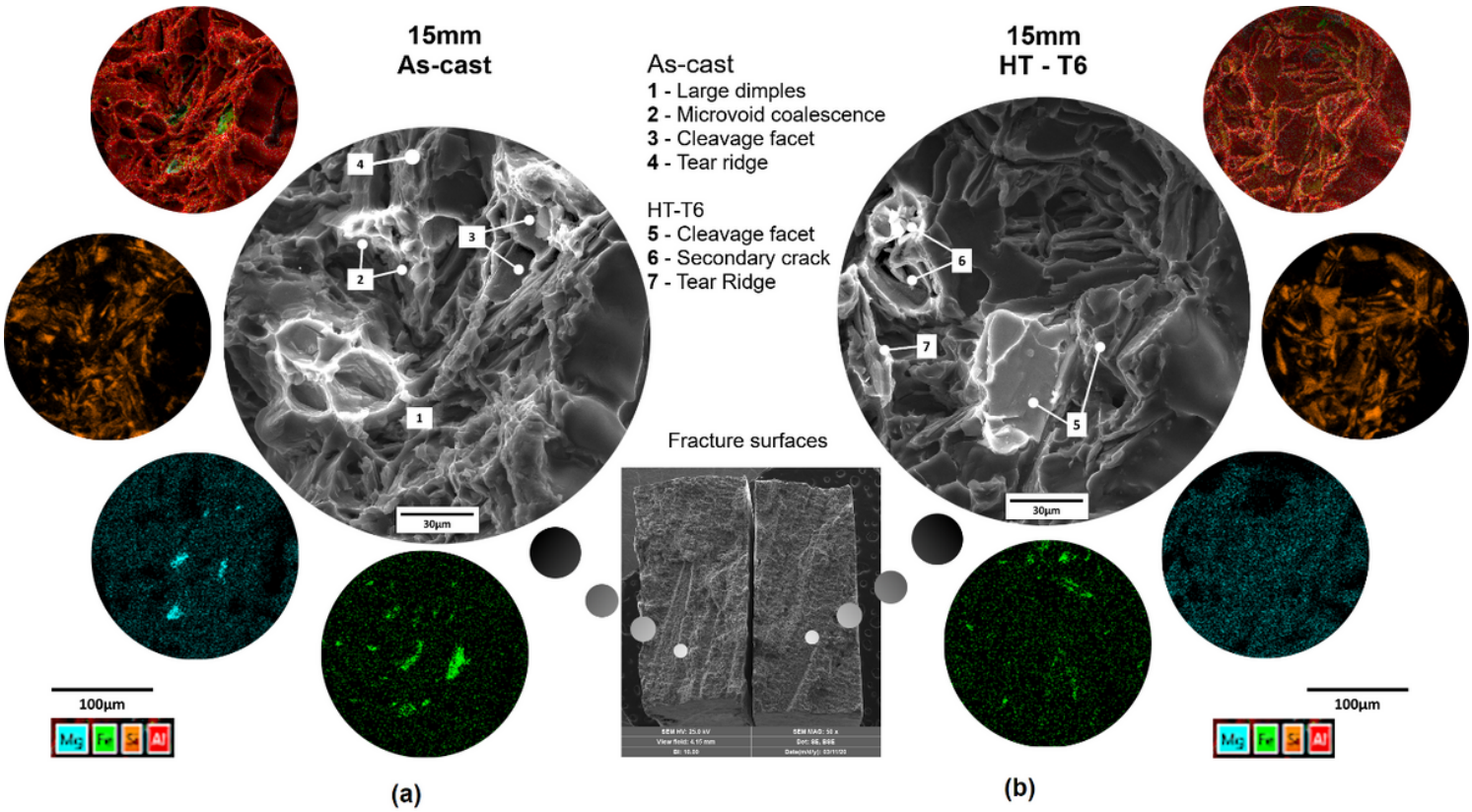

Figure 8

SEM fractographies and elemental scanning mapping by EDS for both investigated samples in the ingot equal to 15mm: (a) as-cast and (b) heat-treated.

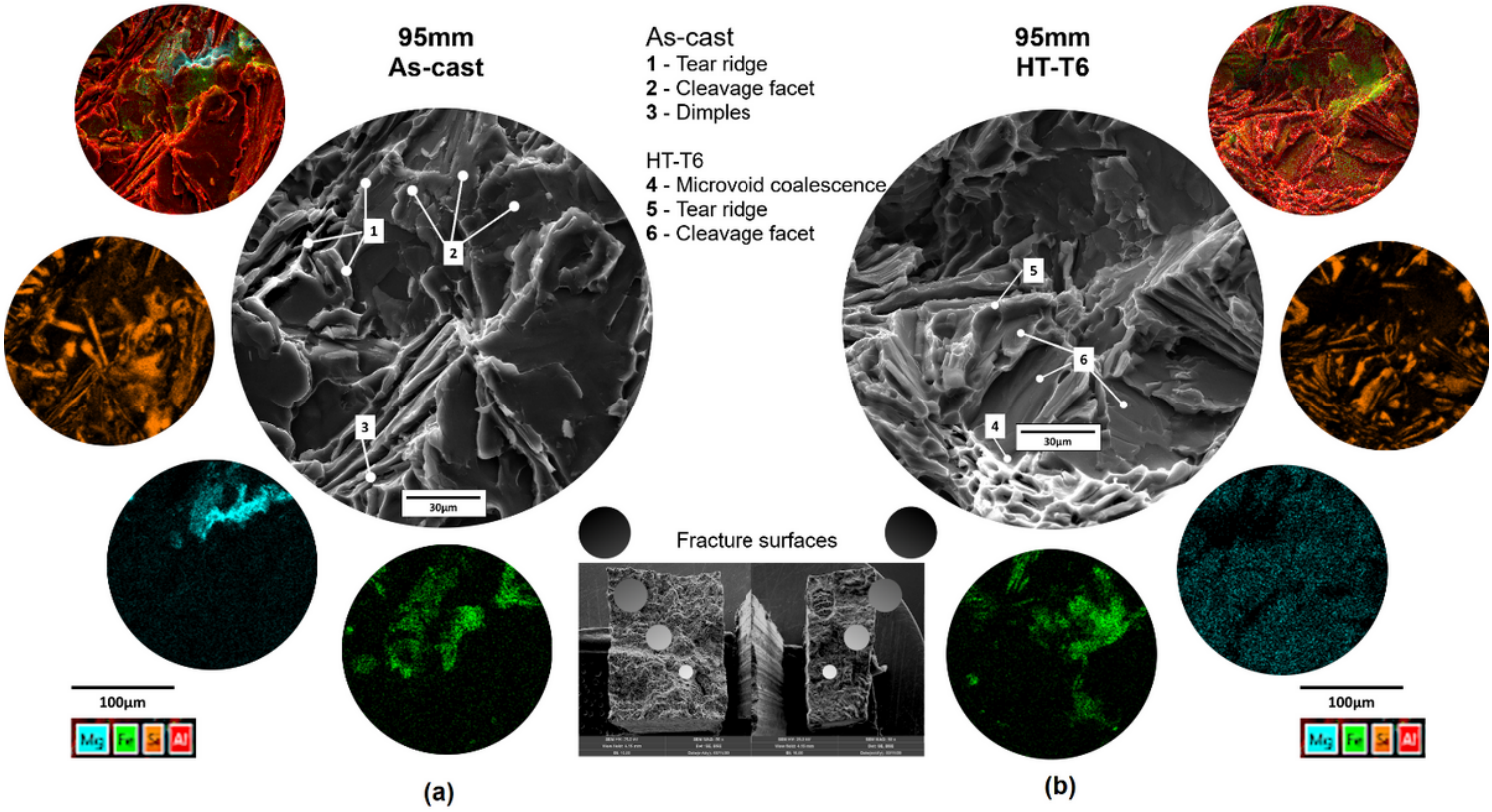

Figure 9

SEM fractographies and elemental scanning mapping by EDS for both investigated samples in the ingot equal to 95mm: (a) as-cast and (b) heat-treated.

Supplementary Files

This is a list of supplementary files associated with this preprint. Click to download.

- GraphicalAbstract.tif